

Harry D. Garner
Kok-Meng Lee*

George W. Woodruff School of Mechanical
Engineering,
Georgia Institute of Technology,
Atlanta, GA 30332-0405

Lin Guo
Maxtor Corporation,
Milpitas, CA 95035

Development of a Grating Interferometer with Application to HDD Servo-Track Writing

The development of a grating interferometer with application to the angular measurement of a hard disk drive actuator arm for application to the servo-track writing process is presented. First, the theoretical background related to the linear type grating interferometer is presented, and this theory is extended to the measurement of the angular displacement of a hard disk drive actuator arm using a linear grating. A vector based diffraction technique has also been developed as a tool for visualization and analysis of the grating interferometer design. Finally, experimental setups and results from a prototype grating interferometer design are presented and discussed to demonstrate the feasibility of the grating interferometer measurement system. [DOI: 10.1115/1.1360694]

1 Introduction

The measurement of nanometer-scale displacements is becoming more common in various high-tech manufacturing processes. One example is in hard disk drive (HDD) servo-track writing (STW). Over the past few decades, the HDD has become the standard form of nonvolatile data storage due to its fast access times and high data density. To store and retrieve data from the disk, there must be a means of measuring the position of the read/write head relative to the disk. This is currently done using servo tracks written onto the disk during the final stages of the manufacturing process. These servo tracks enable the HDD to determine the position of the read/write head and maintain the position over a specific track. The servo-track system acts as an integrated encoder system that makes the high data densities and fast access times of current HDDs possible [1].

Aside from the type of read/write head used and actuator arm resonant frequencies, a fundamental factor that influences the amount of data that can be stored on an HDD is the track density, which is directly related to how closely the servo-tracks can be written. Therefore, the STW operation is a very important aspect of the HDD manufacturing process. The continued increase in track densities by as much as 60 percent per year will rely on the continued increase in the accuracy of the STW process [2].

The actuator arm positioning system of the STW system is one of the critical elements in achieving the highest possible track densities. There are two commonly used approaches to this positioning task known as the mechanical push-pin and optical push-pin. The mechanical push-pin technique uses a push-pin assembly that makes contact with the actuator arm to perform the positioning task. This contact between the actuator arm and push-pin may cause undesirable effects, and misalignments between the push-pin assembly and actuator arm can also cause positioning errors. To maintain contact the STW process must be done in a clean-room environment to prevent contamination of the HDD. The optical push-pin technique uses the voice coil motor of the HDD to position an integrated feature of the actuator arm to track the position of an external optical sensor system mounted to a fine positioning motor [3]. This technique eliminates the need for mechanical contact with the actuator arm because the optical sensor system can act through a transparent window. However, such a system requires two feedback control-loops to control the posi-

tions of the optical sensor system and the HDD actuator arm, and the possibility of misalignment between actuator arm and positioning motor still exists [4].

A fundamental limitation on the track density that can be achieved is related to the accuracy of the measurement system and the positioning of the actuator arm. The mechanical push-pin technique has been found to reduce the track density that can be achieved due to contact between the push-pin and actuator arm. Therefore, a noncontact approach like that of the optical push-pin appears to be the most promising for achieving the highest possible track densities and is currently thought to be the best approach for speed and accuracy in the STW process [5].

From the progression of the two STW approaches, the trend in the measurement of the actuator arm appears to be moving toward a more direct noncontact technique. This is evident in the optical push-pin approach. However, such an approach still requires two feedback control-loops to control the positions of the optical sensor system and the HDD actuator arm. If the need for the second control-loop used to control the optical sensor system could be eliminated while maintaining the measurement capability of the system, the complexity could be reduced which would ultimately result in a reduced cost and an increase in the speed of the STW process. Therefore, a need exists for a less complex system to perform a more direct noncontact measurement of the hard drive actuator arm position that requires only a single feedback control-loop.

In this paper a measurement technique based on the theory of the grating interferometer (GI) will be developed to perform a noncontact direct measurement of the angular displacement of an HDD actuator arm. First, fundamental background related to the operating principle of the GI will be presented. With this background a GI design will be presented that extends the grating interferometer principle to the measurement of the angular displacement of the HDD actuator arm. The expected performance of this design will be examined using a vector-based diffraction technique that provides a means for visualizing the GI configuration. Finally, experimental setups and results designed to verify the feasibility of the GI design will be presented and future enhancements discussed.

2 Grating Interferometer Background

A GI is a type of interferometer that consists of a collimated coherent light source, diffraction grating configuration, and a suitable detector for measuring the phase shift of the interference fringe pattern [6,7]. It can be used to make high-resolution relative

*Corresponding Author. Tel: (404)894-7402; Fax: (404)894-9342; Email: kokmeng.lee@me.gatech.edu

Contributed by the Manufacturing Engineering Division for publication in the JOURNAL OF MANUFACTURING SCIENCE AND ENGINEERING. Manuscript received Nov. 1999; revised April 2000. Associate Editor: E. C. DeMeter.

displacement measurements by relating the phase shift of a fringe pattern to the relative displacement between the light source and the diffraction grating configuration [8].

2.1 Fringe Pattern Determination for Single Grating. To determine the relative displacement between the diffraction grating and light source, the phase shift of the interference fringe pattern must be related to this relative displacement. Figure 1 shows a single grating configuration with a collimated light beam of wavelength λ incident from above. The diffracted orders m_1 and n_1 with angles of diffraction given by θ_{m_1} and θ_{n_1} are shown, and the displacement of the grating, x_1 , is also indicated.

As shown in Fig. 1, where any two diffracted beams from the grating overlap an interference fringe pattern is formed within some region of interference (ROI) with properties determined by the incident beam and the grating. The intensity of this fringe pattern can be determined using fundamental principles of optics by modeling each diffracted beam from the grating as a plane wave traveling in the direction of the diffracted beam including effects from the periodic grating structure [9]. The displacement of the grating causes a phase shift of the diffracted beams given by

$$\phi_m = \frac{2\pi m x_1}{P_1} \quad (1)$$

Equation (1) relates the phase shift of the diffracted order m , the location of Grating 1 (G1), x_1 , and the grating period P_1 [10]. This means that as G1 moves through one of its periods the phase of the m th order diffracted beam will be shifted by $2\pi m$ due to the Doppler shift produced by the moving grating [11]. This relationship is very important because it allows the phase shift of the diffracted beams to be related to the relative motion between the coherent light source and the diffraction gratings making displacement measurement with a GI system possible.

As indicated in Fig. 1, there is an ROI where the m_1 and n_1 diffracted beams overlap. In general, the intensity of the fringe pattern formed in this ROI can be found by taking the modulus squared of the sum of the complex amplitudes of the plane waves present in this ROI. It is straightforward to show that the intensity of this interference fringe pattern is given by

$$I_{m_1 n_1}(x, y) = 2A_{m_1}^2 \left\{ 1 + \cos \left[\frac{2\pi}{P_{D1}} x + \frac{2\pi}{P_{S1}} x_1 + \frac{2\pi}{P_{D1y}} y \right] \right\} \quad (2)$$

with beam amplitudes A_{m_1} assumed real and equivalent and the following periods corresponding to periods of interference fringes in x (P_{D1}) and y (P_{D1y}) directions and period of the fringe phase shift due to grating motion (P_{S1}) have been defined as

$$P_{D1} = \frac{P_1}{n_1 - m_1} = P_{S1} \quad (3)$$

$$P_{D1y} = \frac{\lambda}{\cos \theta_{n_1} - \cos \theta_{m_1}} \quad (4)$$

Equation (2) gives the relationship between the intensity of the fringes and the location of the grating in the x direction. If the

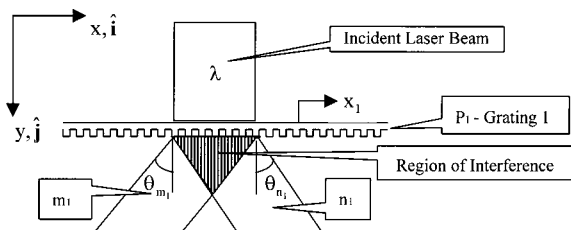


Fig. 1 Grating interferometer with single grating

grating moves, x_1 will change, causing a phase shift of the fringe pattern proportional to the grating displacement. The relation between the fringe pattern phase shift and the grating displacement can be determined by defining the phase of the fringe pattern as the term that depends on the grating displacement, which is

$$\Phi_1 = \frac{2\pi}{P_{S1}} x_1 \quad (5)$$

Equation (5) shows that as G1 moves through a distance P_{S1} the fringe pattern will shift through one of its periods. The G1 displacement corresponding to a particular phase can be found by inverting Eq. (5). In practice, it is useful to consider an incremental displacement due to an incremental phase difference given by

$$\Delta x_1 = \frac{P_{S1}}{2\pi} \Delta \Phi_1 \quad (6)$$

Using Eq. (6) the incremental displacement of G1 can be recovered from an incremental phase shift of the fringe pattern. Equation (2) also shows that as the distance from the gratings increases there will be a phase shift due to the variation of y with an appropriate period. It is interesting to note that P_{D1y} will be infinite when the angle of incidence to G1 is zero. This means that there will be no phase shift as y is varied, which makes such a GI insensitive to out-of-plane displacements.

The resolution of a single grating GI is determined primarily by P_{S1} . For positive and negative first order diffracted beams P_{S1} will be half the grating period. Therefore, the resolution can only be increased by reducing the grating period. In practice, it is not possible to make the grating period arbitrarily small because the size of the detector element used to sample the fringe pattern must be one fourth the period of the fringe pattern. It will be shown in the following sections that a GI system with two gratings can be used to form an interference pattern with a period suitable for some detector element size.

2.2 Dual Grating Configuration. Figure 2 gives a diagram depicting a typical GI with two gratings. This configuration is analogous to that in Fig. 1, but the ROI is now beyond the second grating. It will be shown that the periods of the two gratings can be chosen such that the period of the interference fringes in the ROI will match a specification based on the detector element size. These grating periods will also be shown to be less than that for a single grating case with the same fringe period, which gives an increase in the resolution.

The determination of the intensity of the fringe pattern formed by the dual grating configuration is analogous to the single grating case, but with four diffracted beams determining the characteristics of the interference fringe pattern. Using expressions for the

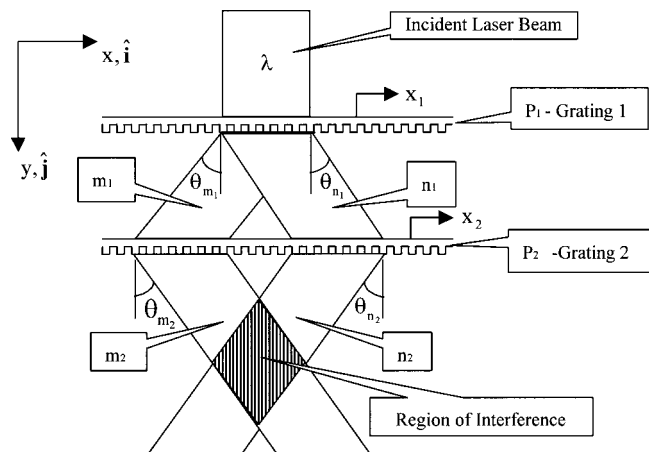


Fig. 2 Grating interferometer with dual gratings

complex amplitudes of the m_2 and n_2 diffracted beams from Grating 2 (G2) including phase shift terms due to G2, the fringe pattern intensity is given by an expression similar to Eq. (2), which can be shown to be

$$I_{m_2 n_2}(x, y) = 2A_{m_2}^2 \left\{ 1 + \cos \left[\frac{2\pi}{P_{D2}} x + \frac{2\pi}{P_{S1}} x_1 + \frac{2\pi}{P_{S2}} x_2 + \frac{2\pi y}{P_{D2y}} \right] \right\} \quad (7)$$

where periods corresponding to periods of the interference fringes in the x (P_{D2}) and y (P_{D2y}) directions and the period of the phase shift of the fringes due to the motion of the gratings (P_{S1} and P_{S2}). The expression for P_{D2y} is analogous to Eq. (4) and P_{D2} , P_{S1} and P_{S2} are given by

$$P_{D2} = \frac{P_1 P_2}{P_1(n_2 - m_2) + P_2(n_1 - m_1)} \quad (8)$$

$$P_{Si} = \frac{P_i}{n_i - m_i} \quad (9)$$

Equation (7) is analogous to Eq. (2), but is in terms of x_1 and x_2 the locations of both gratings. If either grating moves, x_1 or x_2 will change and cause a phase shift of the fringe pattern proportional to the grating displacements. For a typical GI configuration, one grating is fixed with the other allowed to move. With G1 fixed, the phase shift due to motion of G2 is given by

$$\Phi_2 = \frac{2\pi}{P_{S2}} x_2 \quad (10)$$

Equation (10) can be inverted to find the incremental displacement of G2 that corresponds to a particular incremental phase shift analogous to Eq. (6) given by

$$\Delta x_2 = \frac{P_{S2}}{2\pi} \Delta \Phi_2 \quad (11)$$

2.3 Detector Width Compensation. In practice, the detector used to measure the interference fringe pattern has individual elements of a fixed size, and the periods of the diffraction gratings must be chosen to match the detector element size. To recover the phase from the fringe pattern conveniently, it can be shown that the detector element width δ must be one fourth the period of the interference fringes.

For a *single grating* case Eq. (3) will depend on δ to give

$$P_{D1} = 4\delta \quad (12)$$

For the case with positive and negative first-order ($m_1 = +1$ and $n_1 = -1$) beams interfering P_1 is

$$P_1 = 8\delta \quad (13)$$

Substituting Eq. (13) in Eq. (3) gives P_{S1} as

$$P_{S1} = 4\delta \quad (14)$$

This shows the relationship between the detector element size and the period of the phase shift of the fringe pattern. The size of this period is an indication of the resolution that can be obtained with the single grating configuration, and its dependence on δ shows that the resolution can only be increased if δ is reduced. In practice, the detector element size δ is a fundamental limitation that constrains the resolution of a single grating system.

A similar analysis can be done for a *dual grating* configuration. The use of the two gratings acts as a way of compensating for the fact that the detector element width is a fundamental design limitation. With the dual grating configuration, the two gratings must be chosen so that the period of the interference fringes meets a certain criteria. Similar to Eq. (12) the period of interference of the fringe pattern is found from Eq. (8) as

$$P_{D2} = 4\delta \quad (15)$$

Table 1 DWC period combinations with δ multiple

Grating 1 Period (microns)	Grating 2 Period (microns)	Multiple of δ for P_{S2}
20.00	16.00	0.80
45.00	28.80	1.44
48.00	30.00	1.50
80.00	40.00	2.00

As with the single grating case, $m_1 = +1$ and $n_1 = -1$, and $m_2 = -1$ and $n_2 = +1$. This gives Eq. (15) as

$$\frac{P_1 P_2}{2(P_1 - P_2)} = 4\delta \quad (16)$$

For the m_2 and n_2 diffracted beams to overlap, the θ_{m_2} diffracted angle must be positive and the θ_{n_2} diffracted angle must be negative, requiring

$$P_2 < P_1 \quad (17)$$

Equations (16) and (17) are the criteria that must be met by the two grating periods to achieve the detector width compensation (DWC). Unlike Eq. (13) for the single grating case, Eq. (16) is in terms of two grating period values. In practice, the width of the detector elements δ will be a known quantity, and the grating periods satisfying Eq. (16) must be determined. This can be accomplished by iterating over a range of period values and recording period combinations that meet the criteria in Eq. (16). The δ value for the present detector is 10 μm . Table 1 shows grating period combinations that meet the DWC criteria in Eq. (16). Analogous to Eq. (14), the period of the phase shift of the fringe pattern in terms of multiples of the detector element width is also given in Table 1. Compared to the multiple of four in Eq. (14) the values for the DWC configurations are significantly less with the first being less by a factor of five. Therefore, the DWC configuration allows for an increase in the resolution of the GI system using the same size detector because a grating with a smaller period is undergoing displacement.

2.4 Fringe Pattern Analysis. With the intensity distribution of the fringe pattern determined as in Eqs. (2) and (7), it is then possible to relate the phase of the fringe pattern with the displacement of the diffraction gratings as in Eqs. (5) and (10). To recover the phase of the fringe pattern from the intensity distribution it is first necessary to sample the intensity distribution using some type of photosensitive detector. The size of the detector elements plays a role in determining the modulation that occurs on each element as the fringe pattern undergoes phase shifts. A commonly used method for extracting the phase from such a fringe pattern utilizes detector elements with a width one fourth the period of the fringe pattern. This gives four unique signal values phase shifted by ninety degrees with respect to each other, which are known as quadrants. The phase of the fringe pattern can be conveniently recovered using the quadrant values and the inverse tangent function [12]. With the recovered phase, Eqs. (5) and (10) can be used to relate the phase to the grating displacement, and Eqs. (6) and (11) to obtain the incremental displacement.

3 Application of Grating Interferometer to HDD

To use a GI system to measure the angular displacement of an HDD actuator arm, it is necessary to incorporate a reflection type diffraction grating into the arm assembly to induce a phase shift in the diffracted beams formed from the coherent light source that strikes it. The phase shift will then be related to the displacement of the actuator arm so that a measurement can be performed. The relationship between the phase of the fringe pattern formed by the diffracted beams emanating from the arm-mounted grating

and the actuator arm displacement can be derived much like the linear case, but certain important geometrical relationships must be considered.

3.1 Design Geometry. Figure 3 shows the geometry of the arm-mounted grating configuration. In Fig. 3(a) a top view of the actuator arm shows the location of the reflection grating with width W_G . As the arm rotates the effective width of the grating illuminated by the light source will vary as a function of the angle of rotation of the actuator arm θ and is given by

$$W_E = \frac{W_G}{\cos \theta} \quad (18)$$

The light source for the grating interferometer design is a collimated linear laser beam that lies along a line given by $Y = R_L$. It extends over the entire range of motion of the actuator arm to maintain illumination of the grating. As shown in Fig. 3(b), this laser beam is incident to the HDD from above at some angle and passes through a transparent window in the HDD cover and diffracted beams are reflected from the grating to form the fringe pattern. It is also necessary to relate the displacement of the grating along the line illuminated by the light source. The left and right extents of the grating are given by

$$G_{L/R} = R_L \tan \theta \mp \frac{W_G}{2 \cos \theta} \quad (19)$$

With the necessary geometrical relationships for the arm-mounted grating configuration, it is now possible to relate the fringe pattern phase shift and actuator arm displacement. A significant issue related to the grating target is the fact that as the arm rotates the effective period of the grating will vary as a function of the arm

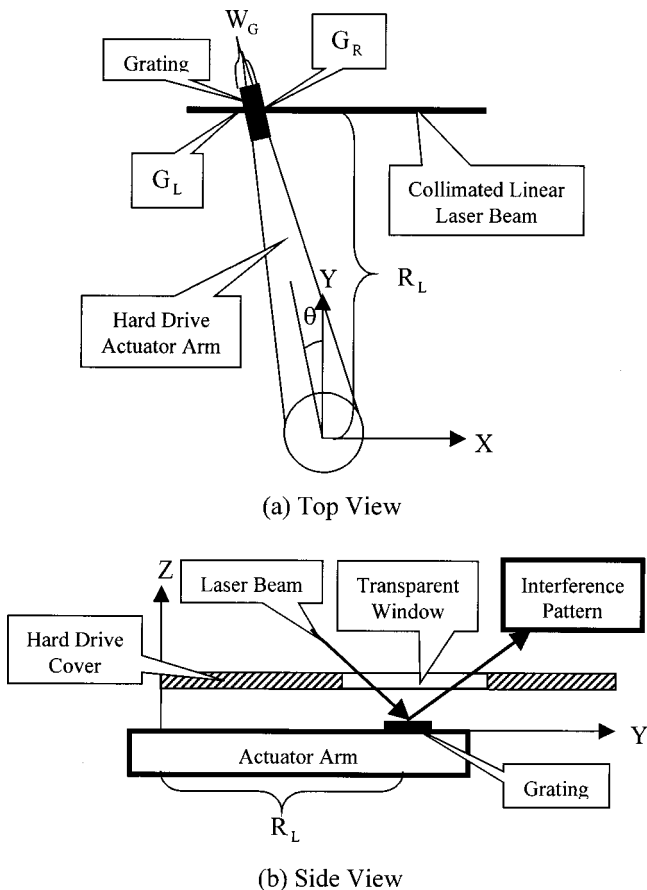


Fig. 3 Actuator arm geometry

orientation. This effective period, P_E , is given in terms of the period of the arm mounted grating P_1 and the arm orientation angle θ as

$$P_E = \frac{P_1}{\cos \theta} \quad (20)$$

The phase shift for an arbitrary diffracted beam can be found by recalling the phase shift term for the linear case from Eq. (1) but with an effective period P_E , and substituting the expression relating the displacement of the grating along the linear light source G_L from Eq. (19) for x_1 gives

$$\begin{aligned} \phi_{m_1}(\theta) &= \frac{2\pi}{P_1} m_1 \left(R_L \tan \theta - \frac{W_G}{2 \cos \theta} \right) \cos \theta \\ &= \frac{2\pi}{P_1} m_1 \left(R_L \sin \theta - \frac{W_G}{2} \right) \end{aligned} \quad (21)$$

This is the orientation dependent phase shift of the m_1 diffracted beam. For positive and negative first orders with $m_1 = +1$ and $n_1 = -1$, the net orientation dependent phase shift of the fringe pattern can be found from the difference between the phase shift of the m_1 and n_1 diffracted beams as

$$\Psi(\theta) = \phi_{m_1}(\theta) - \phi_{n_1}(\theta) = (m_1 - n_1) \frac{2\pi}{P_1} R_L \sin \theta = 2 \frac{2\pi}{P_1} R_L \sin \theta \quad (22)$$

Where the constant phase shift given by the W_G terms has been dropped. Using Eq. (22), the angular displacement can be recovered from the phase of the fringe pattern much like the linear displacement case as discussed in Section 2.4.

3.2 Design Analysis Using Vector Based Diffraction. For design purposes, it is important to be able to visualize the diffracted beams produced from a grating configuration. This is especially useful in determining the placement of the fringe pattern detector and for examining other characteristics of the ROI. To provide such a design tool, a vector based diffraction theory has been developed in which each diffracted beam is fully described in terms of a unit vector in the direction of the diffracted beam and two points which give the left and right extents of the beam. This vector based formulation has been implemented into a recursive diffracted beam ray-tracing routine using MATLAB.

Using the implementation of the vector based diffraction theory, the GI design presented previously can be visualized for analysis. An end view of the arm-mounted grating configuration with a DWC arrangement using two gratings generated using an implementation of the vector based diffraction theory is shown in

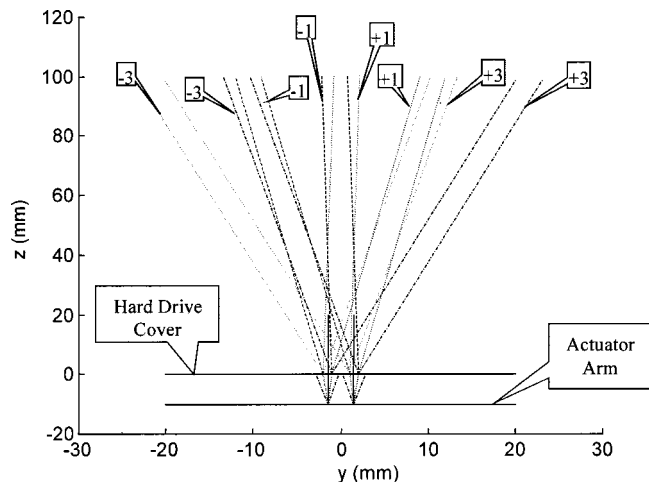


Fig. 4 Arm-mounted grating configuration end view

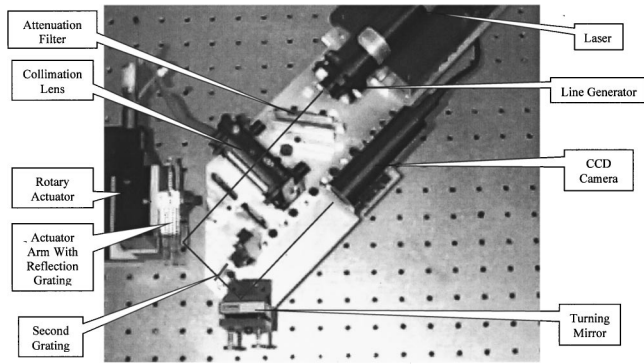


Fig. 5 Top view of rotary stage experimental setup

Fig. 4. The arm-mounted DWC grating has a period of $20\ \mu\text{m}$, and the second grating has a period of $16\ \mu\text{m}$ and is mounted in the cover of the HDD. Because the $20\ \mu\text{m}$ grating is mounted onto the actuator arm, its period must be used when calculating the phase shift due to the arm motion.

Figure 4 shows an end view looking down the central axis of the actuator arm. Planes corresponding to the actuator arm and hard drive cover are indicated. From this figure the diffracted orders emanating from the arm mounted grating and from the second grating in the HDD cover can be seen. Eight diffracted beams are shown that correspond to the set of positive and negative first and third orders emanating from the second grating from the positive and negative first orders reflected from the arm-mounted grating as indicated.

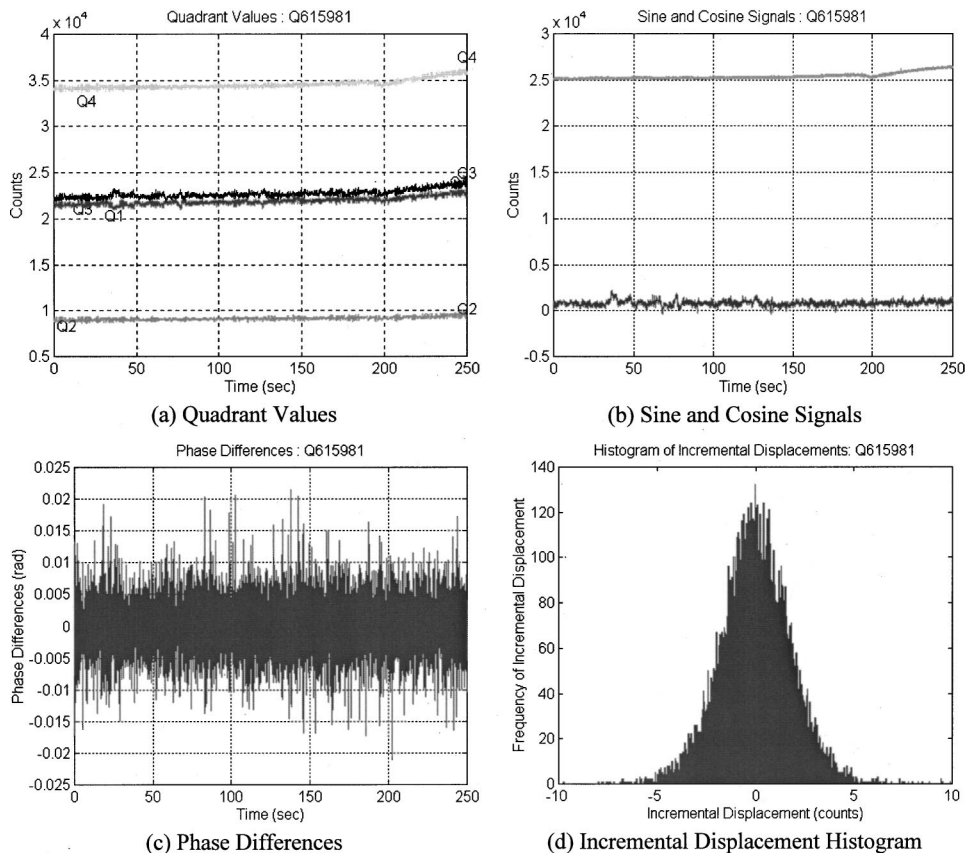


Fig. 6 Results for rotary stage stationary test

4 Experimental Setups and Results

Several experiments have been done to verify the feasibility of the proposed GI design for measuring the angular displacement of an HDD actuator arm. A high-resolution rotary stage with a resolution of 192.3 nanoradians per encoder count has been used to simulate motion of the actuator arm, and the GI design has also been tested with an actual HDD. With these setups stationary and motion tests have been done to demonstrate system stability and motion tracking capability respectively. These experimental setups will now be presented along with corresponding results and discussion.

4.1 Rotary Stage Experimental Setup and Results. Figure 5 shows a top view image of the rotary stage experimental setup, and the components that make up the GI design described in Section 3 can be seen. First, the linear laser beam light source is produced using the combination of the laser, line generator, and cylindrical collimation lens. An attenuation filter is shown which may be necessary to reduce the laser intensity to prevent fringe pattern detector saturation. The linear laser source strikes the reflection grating with $20\ \mu\text{m}$ period fixed to an HDD actuator arm that is mounted to the face of the rotary stage. The reflected diffracted beams pass through the second grating, which is a transmission grating with $16\ \mu\text{m}$ period. The diffracted beams strike a turning mirror and are reflected so that the final overlapping diffracted beams will form the fringe pattern on the fringe pattern detector, which is a CCD camera.

To test the stability of the measurement system, an experiment was done with the rotary stage stationary. Figure 6(a) shows the four quadrant values obtained by summing every fourth row of the fringe pattern detector to obtain four signals with a sinusoidal relationship to the fringe pattern phase and shifted 90 degrees with

Table 2 Statistics from rotary stage stationary test

	Unfiltered Data		Filtered Data	
	(nrad)	(encoder counts)	(nrad)	(encoder counts)
Angular displacement				
Actual	0	0	0	0
Calculated	316.9	1.6474	316.9	1.6474
Incremental Displacement Statistics				
Mean	0.0	0.00014	0.0	0.00014
Standard Deviation	347.4	1.80614	51.7	0.26885

Table 3 Statistics from rotary stage motion test

	Unfiltered Data	Filtered Data
	(encoder counts)	(encoder counts)
Angular Displacement		
Actual	4214	4214
Calculated	4346	~4214
Difference (% Diff)	132 (3.13%)	~0 (~0%)
Radius Value mm(in)	17.85 (0.7027)	18.41 (0.7247)
Incr. Disp. Statistics		
Mean	-0.3596	-0.3487
Standard Deviation	3.1555	0.3566
Counts per Sample	0.3508	

respect to each other. The appropriate differences of the quadrant values will give the sine and cosine of the phase of the fringe pattern as shown in Fig. 6(b) from which the phase can be recovered with the inverse tangent function. The phase differences, which are proportional to the incremental displacements, are shown in Fig. 6(c). An incremental displacement histogram in terms of encoder counts appears in Fig. 6(d). The qualitative information of the histogram is given in Table 2, which shows that the standard deviation of the incremental displacements is within two encoder counts. This standard deviation can be significantly reduced by a low-pass filter. With the aid of Fourier signal analysis, it was found experimentally, that nearly an order of magnitude improvement could be achieved using a low pass filter with a cutoff frequency of 10 Hz. As compared in Table 2, while the mean value remained unchanged the standard deviation was reduced from 347 to 52 nanoradians.

A motion test was performed with the rotary stage moving continuously through 4214 encoder counts to demonstrate the motion tracking capability of the GI system. Figure 7 illustrates the procedure used to recover the displacement measurement from the data obtained from the GI system. Figures 7(a) and 7(b) show the quadrant and sine and cosine values, which are periodic as expected for continuous motion. The recovered phase values appear in Fig. 7(c) and follow a linear trend as expected. Figure 7(d) shows the sine values plotted against the cosine values with a fitted ellipse. It appears that the sine and cosine values fit very closely to an elliptical shape. A histogram of the incremental displacements appears in Fig. 7(e) and most fall within ten encoder counts of zero.

Statistics calculated for unfiltered data from the motion test appear in Table 3. The actual and calculated displacements appear

to vary only by about three percent. This variation is due to the accuracy of the radius value of the light source, noise effects in the detector system, and stability of the intensity of the light source. The mean incremental displacement appears to be quite small, but it has a significant standard deviation.

To reduce the effects of noise in the detector signal, the quadrant values for the motion test were also filtered with a low pass filter. Figure 7(f) shows a histogram of the filtered incremental displacements in terms of encoder counts. Compared to the unfiltered histogram in Fig. 7(e), the filtered values appear to be clearly skewed to the left of zero as would be expected for continuous motion. The shift of the filtered histogram away from zero shows that the effects of the detector noise have been significantly reduced to leave an accurate representation of the motion of the rotary stage as sensed by the detector. Statistics found for the filtered data also appear in Table 3. For the filtered data an optimized radius value was used that reduced the error between the actual and calculated angular displacement values. This optimized radius value was found using Eq. (22) and represents a form of calibration that would be necessary due to the uncertainty in measuring the distance between the laser beam and the axis of rotation. Comparison of the incremental displacement statistics for the unfiltered and filtered data shows that the standard deviation for the filtered case is much less as expected. It is also useful to notice that the mean incremental displacement value compares quite favorably with the counts per sample value, which indicates that the GI system was able to closely track the motion of the rotary stage.

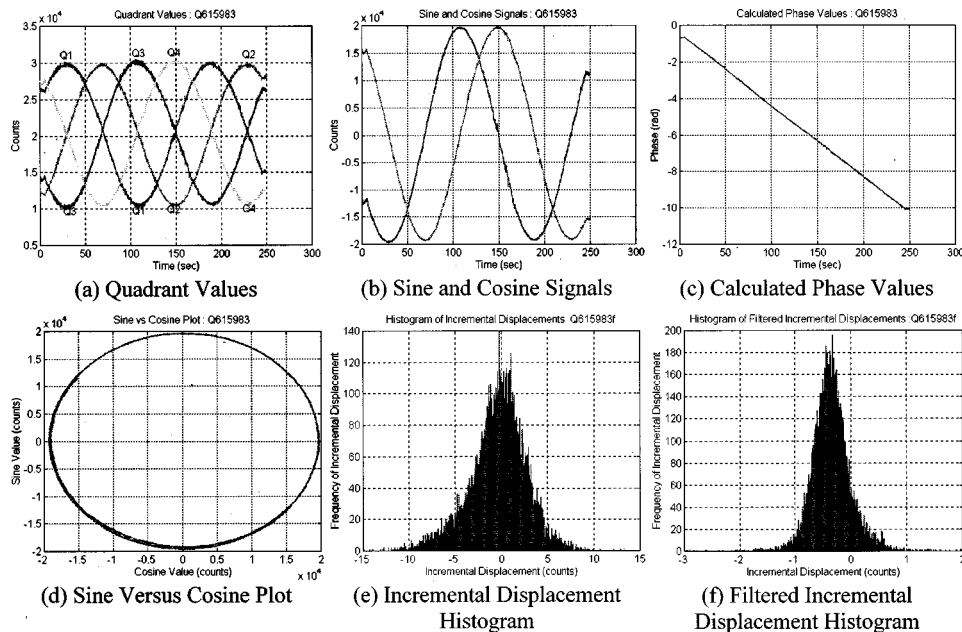


Fig. 7 Results for rotary stage motion test

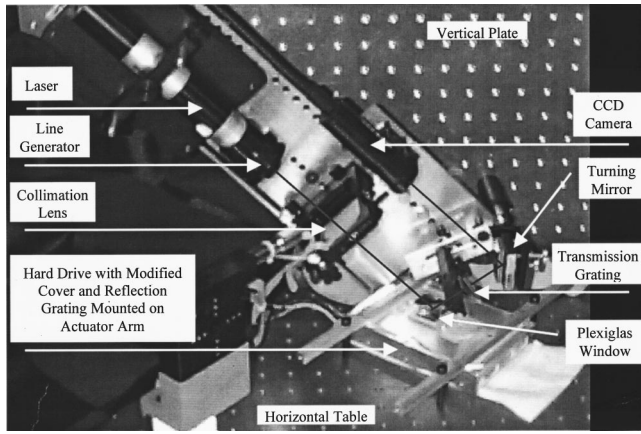


Fig. 8 Image of hard disk drive experimental setup

4.2 Hard Disk Drive Experimental Setup and Results

To verify the capability of the GI system to measure the displacement of an HDD actuator arm, experiments have been done with an actual HDD with a modified cover containing a transparent window and an actuator arm mounted reflection grating. The configuration for such experiments is similar to those just described with the rotary stage, but the mounting plate with the system components was mounted to a vertical plate so that the HDD could remain horizontal. An image of this configuration is shown in Fig. 8.

A stationary test was done with the hard disk drive seeking to a specific track. Figure 9(a) shows the quadrant values that appear to be quite constant as expected for a stationary test aside from noise effects. These quadrant values were also low pass filtered to

Table 4 Statistics from HDD stationary test

	Unfiltered Data		Filtered Data	
Angular displacement	(nrad)	(tracks)	(nrad)	(tracks)
Actual	0	0	0	0
Calculated	8835.7	0.1265	8835.7	0.1265
Incremental Displacement Statistics				
Mean	0.8	0.00001	0.8	0.00001
Standard Deviation	7626.2	0.1092	167.9	0.00240

reduce noise effects as shown in Fig. 9(b). A procedure similar to that described for the rotary stage was done to determine the incremental displacements of the actuator arm.

Statistics found for this stationary test appear in Table 4. The calculated displacement was found to be approximately one tenth of a track, which is quite small. Compared to statistics for the stationary test with the rotary stage shown in Table 2, the incremental displacement statistics appear to be a little more than one order of magnitude greater. This would be caused by the seeking motions of the drive that would lead to less stable stationary signals than with the rotary stage, which would be truly stationary. Table 4 also shows statistics found for the filtered data. The most significant difference between the filtered and unfiltered data is in the standard deviation, which is greater than one order of magnitude less than that from the unfiltered data. This clearly shows the reduction in the variation of the detector signal due to the low pass filtering. The filter may also act to filter out some of the seeking motion of the hard drive.

For the motion test with the hard drive, the drive was commanded to sweep over a range of 10 tracks in one-hundredth (0.01) track increments. For the hard drive tested, 1 track corresponded to an angular displacement of $70 \mu\text{rad}$. The filtered quadrant values obtained from this experiment appear in Fig. 10(a). The filtered sine and cosine signals obtained from the quadrant

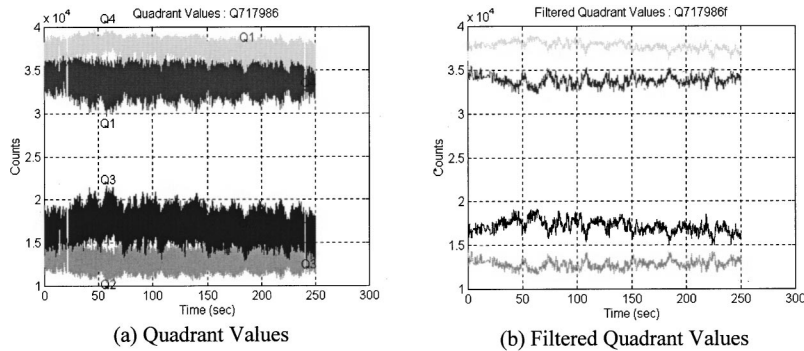


Fig. 9 Results for HDD stationary test

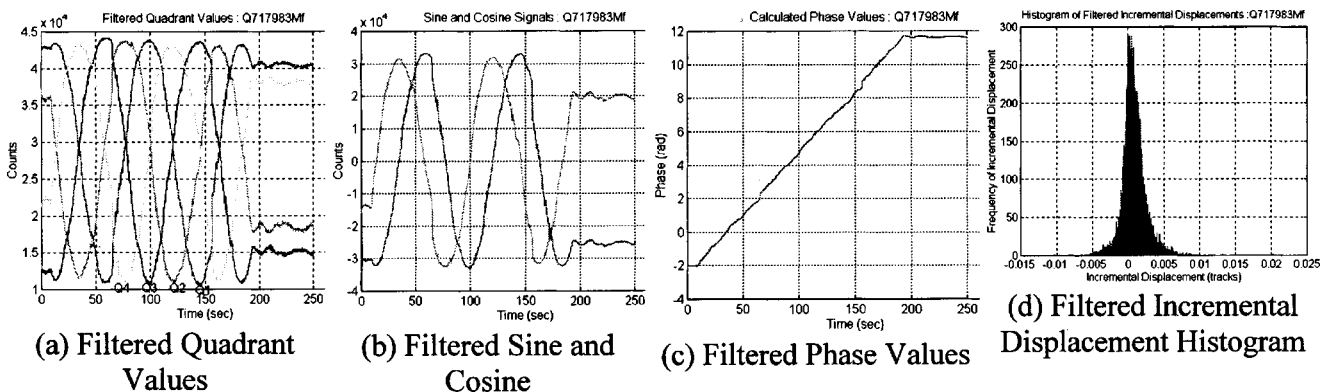


Fig. 10 Results for HDD motion test

Table 5 Statistics from HDD motion test

Angular displacement	Unfiltered Data		Filtered Data	
	(tracks)		(tracks)	
Actual	10		10	
Calculated	9.9959		10	
Difference (% Diff)	0.0041 (0.0406%)		~0 (~0%)	
Radius Value mm(in)	31.31(1.2312)		31.31(1.2312)	
Incr. Disp. Statistics	(nrad)	(tracks)	(nrad)	(tracks)
Mean	77.4	0.001109	77.4	0.001109
Standard Deviation	8105.3	0.116070	142.2	0.002037
Tracks per Sample	0.0011065			

values appear in Fig. 10(b). The recovered phase values appear in Fig. 10(c) and follow a linear trend as expected. Figure 10(d) contains a histogram of the incremental displacements. Careful inspection of this histogram reveals that it is slightly skewed to the right of zero as would be expected for continuous motion.

Statistics found for this hard drive motion test are shown in Table 5. The calculated displacement value agrees very well with the actual displacement due to the use of an optimized radius value, which was only a few percent smaller than the measured value of 1.25 inches. The mean incremental displacement also matches very closely with the number of tracks per sample, which indicates that the GI system was able to follow the motion of the actuator arm very closely. As in the previous data sets, the effect of the low pass filtering on the standard deviation and magnitude statistics can be clearly seen. For the filtered data, these statistics are reduced by more than one order of magnitude.

5 Conclusions and Future Work

An extension of the GI principle to the measurement of the angular displacement of an HDD actuator arm for use in the servo-track writing process has been presented. This GI design has been visualized and analyzed using a vector based diffraction technique. A number of experiments have been done with a prototype of the GI design to demonstrate the feasibility of the measurement system. Experimental results have shown that the system using a CCD camera as a fringe pattern detector is capable of generating stable signals and able to closely track the grating motion. Future enhancements that would be necessary for a production measurement system involve increasing both the measurement resolution and sampling rate. These objectives could be accomplished with either the use of smaller period grating combinations or a photodiode based fringe pattern detector.

Acknowledgments

The research presented in this paper was supported in part by Maxtor Corporation through contract No. E25-A09. The authors would also like to thank DVT, Inc. for providing the CCD camera system used in this research.

Nomenclature

- λ = wavelength of incident light
- θ_m = angle of diffraction of order m diffracted beam

- x_k = grating k displacement
- m_k = diffracted order number m from grating k
- P_k = Grating k period
- ϕ_m = phase shift of diffracted order m due to grating motion
- $I_{m_k n_k}(x, y)$ = intensity distribution of interference fringe pattern due to overlap of m_k and n_k diffracted beams
- A_{m_k} = amplitude of beam of diffracted order m_k
- P_{Dk} = period of interference fringe pattern in x direction for k grating case
- P_{Sk} = period of phase shift of fringe pattern due to grating k motion
- P_{Dky} = period of interference fringe pattern in y direction for k grating case
- Φ_k = grating k displacement dependent fringe pattern phase
- Δx_k = grating k incremental displacement
- $\Delta \Phi_k$ = grating k displacement dependent incremental phase difference
- δ = detector element width
- $G_{L/R}$ = left and right extent of arm mounted grating
- P_E = effective period of arm mounted grating
- R_L = distance of linear laser source from actuator arm rotation axis
- W_E = effective width of arm mounted diffraction grating
- W_G = width of arm mounted diffraction grating
- θ = angle of rotation of hard disk drive actuator arm
- $\Psi(\theta)$ = net actuator arm orientation dependent phase shift of fringe pattern

References

- [1] Lee, C., 1991, "Servowriters: A Critical Tool in Hard Disk Manufacturing," *Solid State Technol.*, **34**, pp. 207–211, May.
- [2] Bajorek, C. H., and Mee, C. D., 1994, "Trends in Storage Technology Through the Year 2000," *Data Storage*, **1**, pp. 23–30, September.
- [3] Horwitz, B., 1996, "Diffractive Techniques Improve Encoder Performance," *Laser Focus World*, **32**, pp. 143–148, October.
- [4] Baker, B., 1996, "Non-Contact Servowriters," Phase Metrics, Inc. Publication, September.
- [5] Freedland, R., 1994, "Laser Interferometry Positions Disk Drive Heads," *Laser Focus World*, **30**, pp. 108–109, December.
- [6] Teimel, A., 1992, "Technology and Applications of Grating Interferometers in High-Precision Measurement," *Precis. Eng.*, **14**, pp. 147–154.
- [7] Kudo, K., Maeda, H., Baba, N., and Funato, H., 1995, "High Resolution Encoder Using Double Gratings," *Proceedings of the SPIE*, **2577**, pp. 138–145.
- [8] Garner, H. D., Lee, K. M., and Guo, L., 1999, "Design Analysis of a Grating Interferometer Sensor for HDD Servo-Track Writing," Submitted to International Conference on Advanced Intelligent Mechatronics (AIM'99) Atlanta, GA, September 1999.
- [9] Bass, M., 1995, *Handbook of Optics*, Vol. 1, 2.5–2.9, McGraw-Hill, New York.
- [10] Parriaux, O., Viorin, G., and Vuillomenet, H., 1995, "Using Conventional Photolithographic Glass Masks as High-Efficiency Phase Gratings," *Opt. Eng.*, **34**, No. 9, pp. 2687–2690.
- [11] Kuo, H.-B., and Lin, J.-D., 1995, "Development of a New Optical Scale System by the Diffractive Phase Interference Method," *Meas. Sci. Technol.*, **6**, pp. 193–196.
- [12] Creath, K., 1988, "Phase-measurement Interferometry Techniques," *Prog. Opt.*, **26**, pp. 349–393.